A Finite Ground Coplanar Line-to-Silicon Micromachined Waveguide Transition

James P. Becker, *Student Member, IEEE*, Yongshik Lee, *Student Member, IEEE*, Jack R. East, *Member, IEEE*, and Linda P. B. Katehi, *Fellow, IEEE*

***Abstract*—Circuits operating in the terahertz frequency range have traditionally been developed using hollow metal waveguides, which, due to the small wavelength at these operating frequencies, must be correspondingly small in cross section. As a result of the high cost of conventional precision machining of such small waveguides, alternate fabrication methods continue to be explored. Silicon micromachining has been suggested as a potential means to produce waveguides in a more cost-effective manner for operation at these frequencies. This paper presents a transition structure that couples the popular finite ground coplanar transmission line to a W-band silicon micromachined waveguide, forming a fully micromachined module. The waveguide is formed via bulk micromachining using a wet etchant, resulting in a diamond cross section. The consequences of utilizing a diamond waveguide in place of the more common rectangular waveguide are considered and potential means of developing rectangular-walled waveguides in silicon are noted. A Ka-band microwave model of a similar transition to a conventional rectangular waveguide is also demonstrated.**

***Index Terms*—Micromachining, millimeter-wave waveguides, silicon, submillimeter-wave waveguides, waveguide transitions.**

I. Introduction

FACTORS such as simplicity of fabrication, its uniplanar nature allowing straightforward integration of series and shunt elements, and relative insensitivity to substrate thickness, make the finite ground coplanar (FGC) transmission line widely used in monolithic microwave integrated circuits (MMICs). However, such lines may be subject to parasitic modes and to radiative and dielectric loss (in addition to conductive loss) at high frequencies. The conventional metal waveguide, on the other hand, still finds significant application due to its ability to transfer high power electromagnetic signals in a low-loss manner. In addition, waveguides may be fashioned into highly directive horn antennas, thus allowing them to be used in transmitting and receiving applications. Unfortunately, waveguides tend to be quite bulky at lower frequencies when compared with planar transmission lines, and difficult and, thus, costly to machine at higher frequencies. The short wavelengths of the terahertz spectrum (broadly defined as the 100-GHz–10-THz frequency range [1]) suggest a favorable combination of the two transmission structures into a single high-density low-cost silicon module.

For example, as was pointed out in [2], a standard rectangular waveguide operating between 140–220 GHz (i.e., a WR-5 waveguide operating in G-band) has cross-sectional dimensions of approximately 1.30 mm in width and 0.65 mm in height. These dimensions are small enough that waveguides could be integrated directly into standard thickness silicon wafers via a micromachining process. Indeed, WR-10 [3] and WR-4 [4] waveguides have been fabricated using (110)-oriented silicon wafers, with measured attenuation of 0.04 and 0.08 dB per wavelength, respectively. In these studies, the fundamental mode was fed to the micromachined waveguides through conventionally machined brass fixtures. In this paper, we present a means to couple to a micromachined guide with a planar transmission line.

While considerable work has been done on microstrip-to-waveguide transitions, comparatively fewer efforts have been made to establish suitable transitions from FGC lines to waveguides [5], [6]. In this paper, we more fully investigate the FGC line-to-silicon diamond waveguide transition that was originally suggested by the authors at the Ninth Topical Meeting on Electrical Performance of Electronic Packaging [7]. Indeed, this paper expands on the original proceedings submission by providing a more complete accounting of the fabrication details of the fully micromachined module, presenting electron micrographs of the structure, and by providing both simulated and measured results of a back-to-back transition.

Prior to presenting the fully micromachined version, a Ka-band microwave model of a similar transition is demonstrated to verify the concept in a manner that was easily measured. This structure combines a conventionally machined rectangular waveguide with a silicon micromachined probe, and is an effective transition spanning the entire band of a WR-28. This design may be scaled to higher frequency bands with the fully micromachined structure using a 90° rotation of the FGC probe.

II. FGC-to-Rectangular-Waveguide Transition

As a starting point to explore E-plane FGC-to-waveguide transitions, a conventionally machined Ka-band rectangular waveguide was employed. A schematic diagram of this Ka-band back-to-back transition is depicted in Fig. 1. The structure consists of an FGC line terminated at each end with a rectangular patch, forming back-to-back probes, which is mounted in conventionally machined metal blocks. The

Manuscript received January 15, 2001. This work was supported by the Defense Advanced Research Projects Agency under Grant N00014-99-1-0915.

J. P. Becker was with the Department of Electrical and Computer Engineering, The University of Michigan at Ann Arbor, Ann Arbor, MI 48109 USA. He is now with the Department of Electrical and Computer Engineering, Montana State University, Bozeman, MT 59717 USA (e-mail: jbecker@ece.montana.edu).

Y. Lee, J. R. East, and L. P. B. Katehi are with the Department of Electrical and Computer Engineering, The University of Michigan at Ann Arbor, Ann Arbor, MI 48109 USA.

Publisher Item Identifier S 0018-9480(01)08689-6.

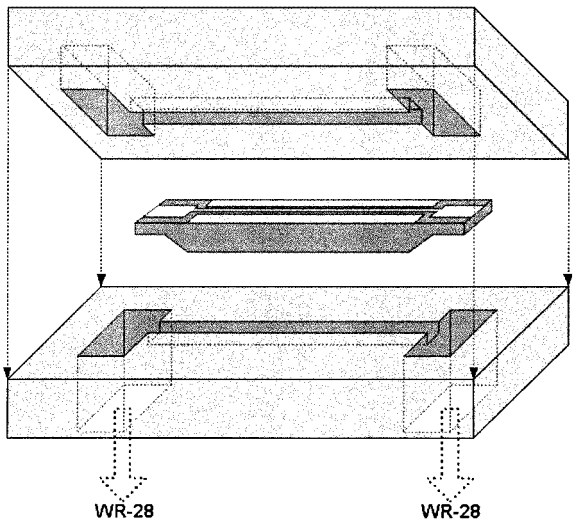

Fig. 1. Schematic diagram of the Ka-band test assembly.

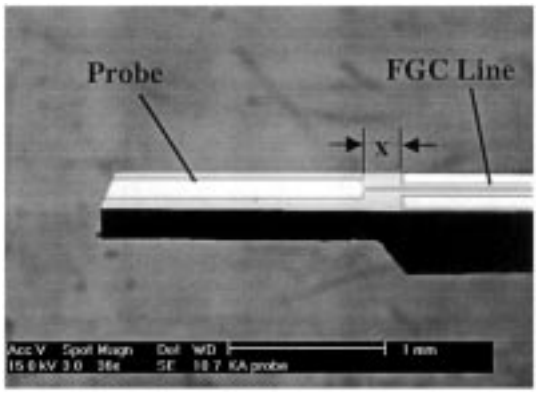

Fig. 2. Scanning electron image of a micromachined probe. The patch and FGC are outlined to improve image clarity.

probe structure (see Fig. 2) was fabricated from 500-μm silicon, with the substrate directly under the patch thinned via wet anisotropic etching to approximately one-half of its original thickness to improve the transition's performance. As suggested in Fig. 1, the probe rests in a shallow groove machined in the metal block, with the height of the groove above the transmission line (which serves as a shield) chosen to ensure single-mode propagation along the line and maintain an impedance of 50 Ω. Each patch faces what becomes the waveguides backshort in the assembled system, with the metal blocks also serving as flanges, accepting WR-28 waveguides, or suitable adapters.

The design of such a transition is based on matching the FGC line (in this case, 50 Ω) to the waveguide using the probes distance to the waveguide backshort ($\sim$2.34 cm), its location in the waveguide cross section ($X = 2.438$ mm), and the patch dimensions (15.950 mm $\times$ 5.436 mm) as matching parameters (see [5] for details).

Measurement of the back-to-back transition was performed using an HP 8510C network analyzer and a pair of HP Q281A coaxial waveguide adapters, with the results given in Fig. 3. The return loss is better than $-$10 dB across the entire waveguide band, with the majority of the band exhibiting better than

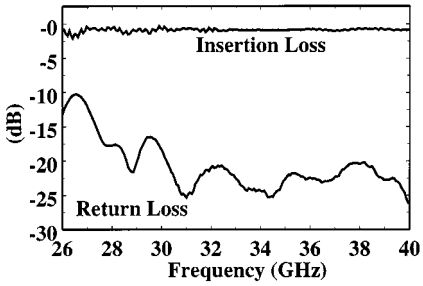

Fig. 3. Measured S-parameters of a back-to-back transition from a rectangular waveguide to an FGC transmission line.

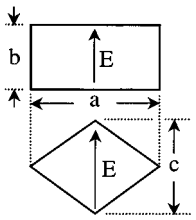

Fig. 4. Cross sections of rectangular and silicon diamond waveguides.

$-$20-dB performance. The insertion loss presented in the figure is that after deembedding the loss of the coaxial adapters and that of the FGC line itself. (The loss of the FGC line was measured through an on-wafer calibration protocol using Multical [8].) Further simulation, not shown here, indicates that simple scaling can be used to produce similar transitions for operation in higher frequency bands. As was mentioned previously, however, conventional machining of metal waveguides and their fixtures for operation at higher frequencies becomes increasing difficult and, thus, costly. For this reason, a silicon micromachined waveguide/FGC line combination was developed.

III. Silicon Diamond Waveguide

In addition to possessing good mechanical, thermal, and electrical properties, the ability to precisely micromachine tiny features in silicon has enabled it to become one of the most important materials in microelectromechanical systems (MEMS). While there are a multitude of techniques used in silicon-based MEMS, bulk anisotropic etching has been a mainstay. This method has been used to micromachine a variety of devices including waveguides [2]–[4]. Here, we investigate the use of a silicon-based waveguide cross section described in [9]–[11] to effect a silicon module that may contain waveguides, planar circuitry, and transitions between the two. Fig. 4 depicts the cross section of a conventional rectangular waveguide and that of the silicon diamond waveguide; the E-field vector of the dominant mode in each guide is suggested in this figure.

The standard rectangular waveguide may be described by cross-sectional dimensions of "a" and "b" where, most commonly, $\mathrm{b} = \mathrm{a}/2$. In the version of the diamond waveguide presented herein, the longer cross-sectional dimension is identical to the "a" dimension of the rectangular guide. The other cross-sectional dimension, i.e., "c," is dictated by the crystal planes of (001)-oriented silicon and has a value of $\mathrm{c} = \mathrm{a}/\sqrt{2}$. It should be noted that in several respects the rectangular waveguide is preferable to the silicon diamond waveguide.

The dimensions of the standard rectangular waveguide ($b = a/2$) are chosen to establish a $2:1$ frequency range of single-mode operation. The single-mode bandwidth of the silicon diamond guide is significantly less, being only approximately $1.33:1$. The advantages of a larger single-mode bandwidth for the rectangular guide are manifested in at least two ways.

The impedance of a given mode in a waveguide becomes purely real at cutoff and decreases with increasing frequency in the case of the dominant TE mode, approaching a value of the characteristic impedance of the medium that fills the guide. By operating a waveguide well above its cutoff frequency, an approximately constant value of impedance is obtained. Since the single-mode bandwidth of the diamond waveguide is substantially less than that of its rectangular counterpart, we expect a greater variation of impedance, as we cannot operate too far from its dominant mode cutoff frequency lest we overmode the guide. Operating a waveguide well above cutoff offers reduced loss as well. Not surprisingly then, the loss (as determined with a commercial full-wave simulation tool[1] assuming a gold metallization of several skin depths) was found to be somewhat larger in the silicon diamond waveguide, being roughly a factor of 1.6 (in decibels per guided wavelength) above that of the rectangular waveguide at 110 GHz.

However, the silicon diamond waveguide has several advantages. As mentioned previously, there are a variety of bulk micromachining technologies in silicon MEMS, which include anisotropic wet etching, reactive ion etching and laser milling. Since anisotropic etching relies on the selectivity of the etchant to crystal orientation, structures defined by crystal planes are realized and are, therefore, potentially very smooth. Sidewall smoothness is of critical importance to optimal performance of a waveguide as its loss may be dominated by surface roughness, with surface imperfections on the order of a skin depth becoming important.

While it is true that anisotropic etching of (110)-oriented silicon reveals vertical sidewalls, the combination of the vertical walls are not rectangular and, thus, a backshort wall will not be perpendicular to the waveguide axis. It should also be mentioned that by introducing metal fins in the diamond waveguide, as described in [11], it is possible to extend the bandwidth of the diamond guide to that of a rectangular waveguide. Our intention here is to demonstrate a transition to an integrated waveguide. In a future study, we intend to take up the possibility of forming rectangular waveguides in silicon via other micromachining techniques, such as deep reactive ion etching (DRIE), and compare their surface roughness to that achieved with the diamond guide.

IV. Fully Micromachined Transition

A. Design

A schematic diagram of the proposed transition from an FGC line to a silicon diamond waveguide is given in Fig. 5. The waveguide is formed in a "split-block" manner by combining two silicon wafers, each which has been anisotropically etched to the depth of $a/2$. (The top wafer is suggested in outline in this figure.) An additional groove has been etched into the bottom half of the guide, with the groove serving to support a probe such as that depicted in Fig. 2. A groove in the top wafer is also etched to act as a shield for the probe. Wet anisotropic etching of the two additional grooves would be problematic due to the severe undercutting that occurs at convex corner during such etching [2] and, thus, DRIE was used.

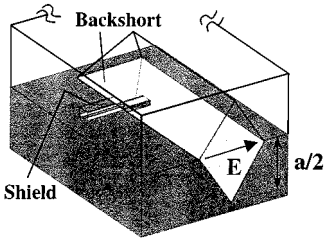

Fig. 5. Schematic diagram of the FGC-to-silicon diamond waveguide transition. A groove is etched in the bottom wafer forming a cradle to accommodate an FGC probe. A shield for the FGC line is etched in the top wafer.

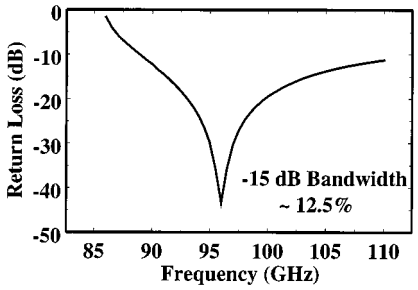

Fig. 6. Simulated results of the return loss of the transition depicted in Fig. 5.

As conceived in the figure, the probe is rotated by 90° with respect to its position as depicted in Fig. 1. Full-wave simulation results have revealed that such a probe rotation made with a transition to a rectangular guide, though requiring different matching parameters, nevertheless allows for operation across the full band of the waveguide. The 90° rotated configuration (i.e., that of Fig. 5) is preferred from a fabrication standpoint in the fully micromachined version.

The full-wave simulation results of the rotated transition to the silicon diamond waveguide are given in Fig. 6. A single transition is found to exhibit a -15-dB bandwidth of $\sim$12.5% and a -10-dB bandwidth greater than 20%. The bandwidth of the transition is considerably less than that possible with a rectangular waveguide and is attributed to the variation in waveguide impedance, as discussed above. (In fact, while the impedance of the appropriate rectangular waveguide varies only by a factor of 1.1 from 90 to 110 GHz, that of the silicon diamond counterpart varies by approximately a factor of 2.1.) Nevertheless, such a transition should be suitable for applications that require bandwidths on the order of 10%.

B. Fabrication

To investigate the possibilities of the FGC-to-silicon diamond waveguide transition, a back-to-back structure consisting of input and output FGC probes feeding a single diamond waveguide was fabricated. The starting material for the top and

[1]Ansoft High Frequency Structure Simulator (HFSS), version 7.0.04, Ansoft Corporation, Pittsburgh, PA.

bottom halves of the waveguide was (001)-oriented high resistivity (>1 k$\Omega\cdot$cm) silicon wafers. Since the waveguides and transition were designed for operation within the W-band (i.e., 75–110 GHz), the "a" dimension of the waveguide (see Fig. 4) was chosen to be that of a conventional WR-10, specifically 2.54 mm. To realize the waveguide in the split-block method suggested in Fig. 5, and to provide adequate mechanical stability of the etched structure, a wafer thickness of 2 mm was chosen. A thermal oxide approximately 8000-Å thick was grown on the bare wafers to serve as a masking layer.

Rectangular apertures for subsequent anisotropic etching of the waveguide halves were opened in the oxide via standard photolithography and chemical etching using buffered hydrofluoric acid. The remaining oxide then served as a masking layer for wet anisotropic etching of the waveguide grooves. 25% tetramethyl ammonium hydroxide (TMAH) was chosen for anisotropic etching due to its ability to realize extremely smooth sidewalls. Unfortunately, the $(001)/(111)$ selectivity is not as great with TMAH as it is with other wet anisotropic etchants such as potassium hydroxide and, thus, mask undercutting had to be taken into account. The etch rate was approximately 20 μm/h and the $(001)/(111)$ selectivity taken to be 10/1. After wet anisotropic etching, the oxide mask was stripped.

Photoresist was then used as a masking layer for etching of both the cradles (i.e., additional groove on the bottom wafer) used to hold the micromachined probes and the transmission line shields (etched on the top wafer). Applying photoresist to micromachined structures via typical wafer spinning is a troublesome proposition in that the applied resist may be far from uniform. A nonuniform resist coating leads to difficulty in properly resolving features photolithographically and to providing adequate protection to underlying layers where photoresist is to serve as an etch mask. A means to employ electrodeposition of photoresist has been explored by the authors [2], [12] and largely mitigates the problems encountered in resist spinning on micromachined structures. In future iterations of the work presented here, we intend to introduce electrodeposited resist into the fabrication process, but have for the present used conventional wafer spinning to apply photoresist. Roughly 7 μm of resist served as the etch mask for DRIE of the probe cradles and shields.

The DRIE system used is a Surface Technology Systems (STS) tool that employs a time-multiplexed process [13] to etch silicon. The etching process is carried out by cycling between two repeating steps. The first step involves the deposition of a thin fluorocarbon film, which is immediately followed by the second step, i.e., reactive ion etching of a shallow trench. By properly adjusting the passivation and etch times, gas flow, and applied RF power, a variety of etch profiles are possible. The process utilized in this study consisted of a seven second passivation step using C_4F_8 and a 13-s etch step using SF_6, which yielded profiles approximately 5° from vertical. The etch rate, which depends upon the exposed area and pattern dimensions, was approximately 6 μm/min for the structures developed here and, thus, etching a depth of 100 μm (the thickness of the probe insert) required approximately 17 min of cycling through the passivation and etching steps.

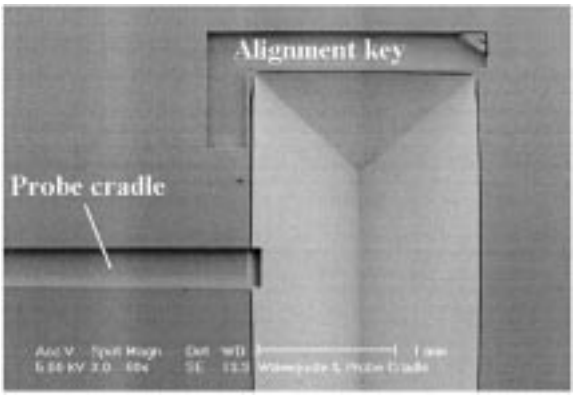

Fig. 7. Scanning electron micrograph of the bottom half of the micromachined waveguide in plan view.

After deep etching, the protective resist layer was removed using acetone and the wafer cleaned in a "Piranha" etch consisting of a 1 : 1.2 mixture of 30% hydrogen peroxide and sulfuric acid for 10 min. The wafer was then coated with a sputtered bilayer of 1000 Å of titanium, which served as an adhesion layer, followed by a 1.6-μm-thick layer of gold. A scanning electron micrograph of the micromachined structure (prior to metallization) is given in Fig. 7. It is interesting to note that the alignment key was not entirely etched, as a small silicon island exists in one corner of the key. This small island is due to incomplete removal of the photoresist mask prior to deep etching and is evidence of the potential difficulties arising from spinning resist on micromachined surfaces. Another deleterious effect of wafer spinning of the resist is evident in the thin etched groove that surrounds the waveguide. The resist tends to be quite thin on the immediate edge of a micromachined cavity or groove, a problem that is exacerbated by reflow occurring during resist soft baking. To attempt to solve these problems, we intend to use the electrodepositable resist previously mentioned.

The FGC probes used in the fully micromachined module were fabricated using 100-μm-thick high-resistivity ($\rho > 2000\ \Omega\cdot$cm) bare silicon wafers. The metallization pattern was formed on the top surface using a bilayer of chromium (500 Å) and gold (1 μm) in a standard liftoff process. The FGC line had signal, slot, and ground strip widths of 36, 30, and 114 μm, respectively. The etching pattern was formed on the backside of the wafer and properly registered to the top surface using infrared alignment. The patterned wafer was then mounted upside down on a carrier wafer and micromachined using the STS system until the 100-μm wafer was etched entirely through. The probes were then released in acetone and thoroughly cleaned.

A schematic drawing of an etched FGC probe is given in Fig. 8. Arm-like appendages were developed on the probes (the probe cradles on the lower waveguide wafer had the identical arms) to ensure that the probes would not shift when placed in the probe cradle. Finally, Fig. 9 displays a photomicrograph of a probe that has been inserted into the bottom half of a waveguide. Again, incomplete etching of the alignment key is evident. The pits visible in the lower left-hand-side corner of the micrograph were wet etched in TMAH and were introduced to accommodate the National lnstitute of Standards (NIST), Boulder, CO,

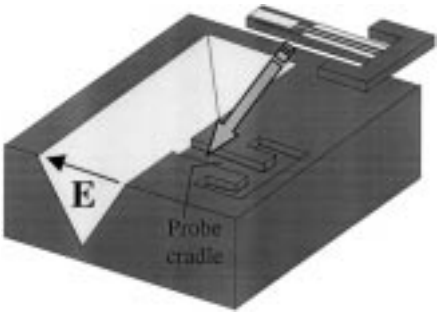

Fig. 8. Schematic diagram of an etched FGC probe and probe cradle.

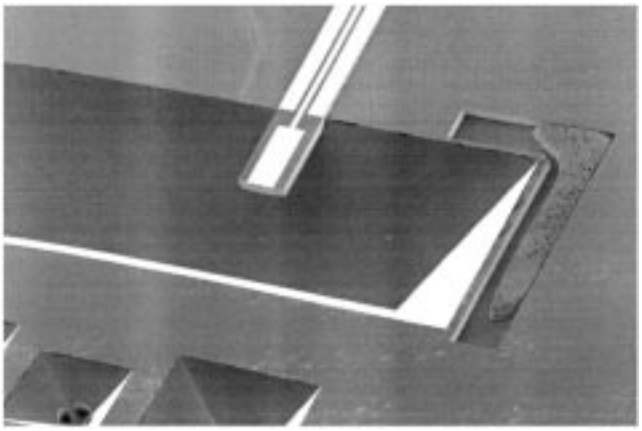

Fig. 9. Scanning electron micrograph of the bottom half of the micromachined waveguide with an FGC probe inserted into its cradle.

traceable glass microspheres. Similar pits were etched in the top half of the guide, thus allowing simple alignment of the top and bottom halves of the waveguide.

V. Measured Result

A back-to-back transition consisting of input and output FGC lines with a short section of diamond waveguide (0.7 cm) in between was measured in W-band using an HP 8510C vector network analyzer and a set of ground–signal–ground model 120 GGB picoprobes. Calibration was achieved with a thru-reflect-line (TRL) protocol [8], using on-wafer thru, short, and delay lines. The reference planes were moved to the point on the feed lines at which they met the waveguide. The simulated and measured results of a back-to-back transition are given in Fig. 10.

The loss due to propagation in the waveguide was predicted using full-wave simulation and has been removed from the displayed data. In another study [14], an assumed metal conductivity of 5.0×10^6 $(\Omega\cdot\text{m})^{-1}$ was found to provide good agreement between measured and simulated performance of our diamond waveguides and, thus, was used here. The loss of the section of diamond waveguide should be small, and is predicted, for instance, to be -0.17 dB at 100 GHz. The simulation results shown in Fig. 10 are for the lossless case.

The fact that the structure's transmission characteristic does not increase as rapidly as the simulation predicts is due at least in part to the fact that the fabricated waveguide was somewhat smaller than designed, thus moving the waveguide's cutoff

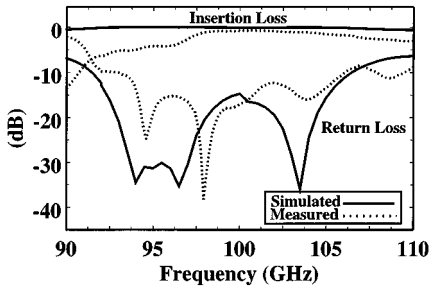

Fig. 10. Simulated and measured results of a back-to-back FGC to silicon diamond waveguide transition.

frequency somewhat higher. The -10-dB bandwidth of the back-to-back transition is approximately 13%, roughly what is expected. From 98 to 102 GHz, the transition performs reasonably well with a measured insertion loss per transition less than 0.45 dB. It is believed that the performance of the transition will be significantly improved with elimination of such imperfections as the thin etched groove that surrounds the guide and through use of thermo-compression bonding of the waveguides (the waveguide halves were clamped in this study).

VI. Conclusion

A transition from an FGC transmission line to a silicon micromachined waveguide has been studied in this paper. Diamond-shaped waveguides for operation near 100 GHz were developed using anisotropic wet etching by revealing (111) crystal planes in (001)-oriented silicon wafers. A DRIE system was used to micromachine both FGC probes and grooves abutting the waveguide used to house and shield the probes. The measured -10-dB return-loss bandwidth of a back-to-back transition was found to be roughly 13%, with a loss per transition of less than 0.45 dB from 98 to 102 GHz. Fine tuning of the fabrication protocol, as well as investigation of alternate micromachining techniques to develop rectangular waveguides, is underway.

The transition structure presented here required manual assembly of the probe and waveguide combination, which becomes more difficult as the size of the components shrink. One potential means to address this difficulty for higher frequency designs is to maintain the size of the precisely micromachined probe cradle and only reduce the size of the printed portions of the probe. That is, the FGC line and patch metallization would be patterned photolithographically (as is currently done) to the reduced dimensions required by the operating frequency, yet the supporting structure would remain of suitable size for handling. The supporting substrate would naturally need to be made thin enough to avoid parasitic effects; we are currently investigating various membrane structures for just such a purpose.

If just a single waveguide transition or two is required for a given module, conventional machining of the waveguide may be the proper choice. If many waveguides and transitions are to be developed in a single module, for a power-combining array, for instance, and/or hundreds of modules are to be produced, the advantages of batch fabrication may make a silicon-based waveguide process preferred.

Finally, it should be noted that silicon micromachining is just one of the techniques being investigated to develop miniature

waveguides for terahertz frequencies. For example, other investigations have produced reduced-height waveguides at W-band using a "snap together" technology based on a negative photoresist (EPON SU-8) [15], and an X-ray lithographie, galvanoformung, abformuna (LIGA) technique has been used to fabricate a 2.5-THz package [16], [17], though no measured results are given in the X-ray LIGA work. Clearly, the challenge of developing low-cost high-performance terahertz guiding structures remains an area of research interest and is being addressed in a variety of unique manners.

ACKNOWLEDGMENT

The authors thank Dr. K. Najafi, The University of Michigan at Ann Arbor, and P. Sunal, The University of Michigan at Ann Arbor, for their helpful discussions on the deep etching system, Dr. G. Rebeiz, The Univesity of Michigan at Ann Arbor, for his insights on terahertz micromachining, and the reviewers for their thoughtful comments and suggestions.

REFERENCES

[1] F. T. Ulaby, "Scanning the issue, terahertz technology," *Proc. IEEE*, vol. 80, pp. 1659–1661, Nov. 1992.
[2] J. P. Becker and L. P. B. Katehi, "Toward a novel planar circuit compatible silicon micromachined waveguide," in *Proc. IEEE 8th Elect. Performance Electron. Packag. Topical Meeting* , Oct. 1999, pp. 221–224.
[3] W. R. McGrath, C. Walker, M. Yap, and Y.-C. Tai, "Silicon micromachined waveguides for millimeter-wave and submillimeter-wave frequencies," *IEEE Microwave Guided Wave Lett.*, vol. 3, pp. 61–63, Apr. 1993.
[4] V. M. Lubecke, K. Mizuno, and G. Rebeiz, "Micromachining for terahertz applications," *IEEE Trans. Microwave Theory Tech.*, vol. 46, pp. 1821–1831, Nov. 1998.
[5] E. Tentzeris *et al.*, "FDTD characterization of waveguide probe structures," *IEEE Trans. Microwave Theory Tech.*, vol. 46, pp. 1452–1460, Oct. 1998.
[6] G. E. Ponchak and R. N. Simons, "A new rectangular waveguide to coplanar waveguide transition," in *IEEE MTT-S Int. Microwave Symp. Dig.*, vol. 1, 1990, pp. 491–492.
[7] J. P. Becker, Y. Lee, J. R. East, and L. P. B. Katehi, "A fully packaged finite-ground coplanar line-to-micromachined waveguide transition," in *Proc. IEEE 9th Elect. Performance Electron. Packag. Topical Meeting*, Oct. 2000, pp. 273–276.
[8] R. B. Marks and D. F. Williams, "De-embedding software," in *Program Multical, Version 1.0*. Boulder, CA: NIST, 1995.
[9] B. Shenouda, L. W. Pearson, J. E. Harriss, W. Wang, and Y. Guo, "Etched silicon micromachined waveguides and horn antennas at 94 GHz," in *IEEE AP-S Int. Symp. Dig.*, vol. 2, 1996, pp. 988–991.
[10] B. Shenouda and L. W. Pearson, "Micromachined waveguide for millimeter wave applications," in *Proc. Int. Microwave Millimeter-Wave Technol.Conf.*, 1998, pp. 615–618.
[11] B. A. Shenouda, L. W. Pearson, and J. E. Harris, "Etched-silicon micromachined W-band waveguides and horn antennas," *IEEE Trans. Microwave Theory Tech.*, vol. 49, pp. 724–727, Apr. 2001.
[12] J. P. Becker and L. P. B. Katehi, "Multilevel finite ground coplanar line transitions for high-density packaging using silicon micromachining," in *Proc. IEEE MTT-S Int. Microwave Symp. Dig.*, vol. 1, 2000, pp. 303–306.
[13] A. A. Ayón, "Time-multiplexed deep etching," *Sens. Mag.*, vol. 17, no. 8, pp. 64–69, Aug. 2000.
[14] J. P. Becker, "Silicon micromachined waveguide transitions and three-dimensional lithography for high-frequency packaging," Ph.D. dissertation, Dept. Elect. Eng. Comput. Sci., Univ. Michigan at Ann Arbor, Ann Arbor, MI, 2001.
[15] C. E. Collins *et al.*, "A new micro-machined millimeter-wave and terahertz snap-together rectangular waveguide technology," *IEEE Microwave Guided Wave Lett.*, vol. 9, pp. 63–65, Feb. 1999.
[16] S. W. Moon *et al.*, "Terahertz waveguide components fabricated using 3D X-ray microfabrication technique," *Electron. Lett.*, vol. 32, no. 19, pp. 1794–1795, Sept. 1996.
[17] I. C. E. Turcu *et al.*, "X-ray micro- and nanofabrication using a laser-plasma source at 1 nm wavelength," *J. Vac. Sci. Technol.*, vol. B 15, no. 6, pp. 2495–2502, 1997.

James P. Becker (S'98) received the B.S. degree in ceramic engineering from the University of Illinois at Urbana-Champaign, in 1992, the M.S.E.E degree from Colorado State University, Fort Collins, in 1995, and the Ph.D. degree in electrical engineering from The University of Michigan at Ann Arbor, in 2001.

He is currently with the Department of Electrical and Computer Engineering, Montana State University, Bozeman. His current research interests include silicon micromachining for high-frequency applications, RF/microwave circuitry, and silicide-based infrared detectors.

Yongshik Lee (S'00) was born in Seoul, Korea. He received the B.S. degree from Yonsei University, Seoul, Korea, in 1998, the M.S. degree from The University of Michigan at Ann Arbor, in 2001, and is currently working toward the Ph.D. degree in electrical engineering and computer science at The University of Michigan at Ann Arbor.

His current research interests include monolithic microwave/millimeter-wave integrated circuits and silicon micromachining for high-frequency applications.

Jack R. East (S'70–M'72) received the B.S.E., M.S., and Ph.D. degrees from The University of Michigan at Ann Arbor, in 1969, 1970, and 1986, respectively.

He is currently with the Solid-State Electronics Laboratory, The University of Michigan at Ann Arbor, where he conducts research in the areas of high-speed microwave device design, fabrication and experimental characterization, nonlinear device and circuit modeling, and terahertz technology.

Linda P. B. Katehi (S'81–M'84–SM'89–F'95) received the B.S.E.E. degree from the National Technical University of Athens, Athens, Greece, in 1977, and the M.S.E.E. and Ph.D. degrees from the University of California at Los Angeles, in 1981 and 1984, respectively.

In September 1984, she joined the faculty of the Electrical Engineering and Computer Science Department, The University of Michigan at an Arbor, as an Assistant Professor, and then became an Associate Professor in 1989 and Professor in 1994. She has served in many administrative positions, including Director of Graduate Programs, College of Engineering (1995–1996), Elected Member of the College Executive Committee (1996–1998), Associate Dean For Graduate Education (1998–1999), and Associate Dean for Academic Affairs (since September 1999). She has authored or co-authored 410 papers published in refereed journals and symposia proceedings and she holds four U.S. patents. She has also generated 20 Ph.D. students.

Dr. Katehi is a member of the IEEE Antennas and Propagation Society (IEEE AP-S), the IEEE Microwave Theory and Techniques Society (IEEE MTT-S), Sigma Xi, Hybrid Microelectronics, and URSI Commission D. She was a member of the IEEE AP-S AdCom (1992–1995). She was an associate editor for the IEEE TRANSACTIONS ON MICROWAVE THEORY AND TECHNIQUES and the IEEE TRANSACTIONS ON ANTENNAS AND PROPAGATION. She was the recipient of the 1984 IEEE AP-S W. P. King (Best Paper Award for a Young Engineer), the 1985 IEEE AP-S S. A. Schelkunoff Award (Best Paper Award), the 1987 National Science Foundation Presidential Young Investigator Award, the 1987 URSI Booker Award, the 1994 Humboldt Research Award, the 1994 University of Michigan Faculty Recognition Award, the 1996 IEEE MTT-S Microwave Prize, the 1997 International Microelectronics and Packaging Society (IMAPS) Best Paper Award, and the 2000 IEEE Third Millennium Medal.